Howard Hughes Medical Institute

Published as: *Nat Genet*. 2019 January ; 51(1): 42–50.

ROBO4 Variants Predispose Individuals to Bicuspid Aortic Valve and Thoracic Aortic Aneurysm

Russell A Gould[#1,2], **Hamza Aziz**[#1,2], **Courtney E Woods**[#1], **Manuel Alejandro Seman-Senderos**[1], **Elizabeth Sparks**[1], **Christoph Preuss**[3,4], **Florian Wünnemann**[3], **Djahida Bedja**[5,6], **Cassandra R Moats**[5,7], **Sarah A McClymont**[8], **Rebecca Rose**[1], **Nara Sobeira**[1], **Hua Ling**[8], **Gretchen MacCarrick**[1], **Ajay Anand Kumar**[9], **Ilse Luyckx**[9], **Elyssa Cannaerts**[9], **Aline Verstraeten**[9], **Hanna M Björk**[10], **Ann-Cathrin Lehsau**[11], **Vinod Jaskula-Ranga**[12], **Henrik Lauridsen**[13], **Asad A Shah**[14], **Christopher L Bennett**[1,2], **Patrick T Ellinor**[15,16], **Honghuang Lin**[17], **Eric M Isselbacher**[18], **Christian Lacks Lino Cardenas**[19], **Jonathan T Butcher**[13], **G. Chad Hughes**[20], **Mark E. Lindsay**[21], **Center for Mendelian Genomics**[22], **MIBAVA Leducq Consortium**[22], **Luc Mertens**[23], **Anders Franco-Cereceda**[24], **Judith MA Verhagen**[25], **Marja Wessels**[26], **Salah A Mohamed**[11], **Eriksson Per**[10], **Seema Mital**[26], **Lut Van Laer**[9], **Bart L Loeys**[9,27], **Gregor Andelfinger**[4,28], **Andrew S McCallion**[#,1,5,30], and **Harry C Dietz**[#,1,2,29,30]

[1]McKusick-Nathans Institute of Genetic Medicine, Johns Hopkins University School of Medicine, Baltimore, Maryland, USA [2]Howard Hughes Medical Institute, Baltimore, Maryland, USA [3]Cardiovascular Genetics, Department of Pediatrics, Centre Hospitalier Universitaire Sainte-Justine Research Centre, Université de Montréal, Montreal, Quebec, Canada [4]The Jackson Laboratory, Bar Harbor, Maine, USA [5]Department of Molecular and Comparative Pathobiology, Johns Hopkins University School of Medicine, Baltimore, Maryland, USA [6]Heart and Vascular Institute, Division of Cardiology, Johns Hopkins University School of Medicine, Baltimore, Maryland, USA [7]Oregon National Primate Research Center, Portland, Oregon, USA [8]Center for Inherited Disease Research, Johns Hopkins University School of Medicine, Baltimore, Maryland, USA [9]Center for Medical Genetics, Faculty of Medicine and Health Sciences, Antwerp University Hospital and University of Antwerp, Antwerp, Belgium [10]Center for Molecular Medicine, Department of Medicine Solna, University hospital Solna, Karolinska Institutet, Stockholm, Sweden [11]Department of Cardiac and Thoracic Vascular Surgery, University Hospital Lübeck,

[#]Denotes equal co-corresponding author.

AUTHOR CONTRIBUTIONS

H.C.D., B.L.L., G.A., and the MIBAVA Leducq Consortium recruited participants for the study. A.S.M., H.C.D., G.A., and B.L.L. were instrumental in the experimental design and interpretation of the data. R.A.G. and M.A.S.S. performed in vitro experiments and R.A.G. performed mouse experiments with assistance from D.B. under the supervision of H.C.D. C.E.W. performed all zebrafish experiments with assistance from C.R.M., R.R., and S.A.M. under the supervision of A.S.M. The initial mouse studies, genetic analysis, and identification of the gene of interest were performed by H.A. under the supervision of H.C.D.

COMPETING FINANCIAL INTERESTS

The authors declare no competing financial interests.

DATA AVAILABILITY

ROBO4 variants were submitted to ClinVar (https://www.ncbi.nlm.nih.gov/clinvar/) and have the following accession codes: SCV000804228, SCV000804229, SCV000804230, SCV000804231, SCV000804232, SCV000804233, SCV000804234, SCV000804235, SCV000804236, SCV000804237, SCV000804238, SCV000804239. Exome sequencing data is not publicly available due to consent restrictions.

Lübeck, Germany [12]Wilmer Eye Institute in the Department of Ophthalmology at the Johns Hopkins University School of Medicine, Baltimore, Maryland, USA [13]The Nancy E. and Peter C. Meinig School of Biomedical Engineering, Cornell University, Ithaca, New York [14]Rex Hospital, Raleigh, North Carolina [15]The Broad Institute of MIT and Harvard, Cambridge, MA, USA [16]Cardiovascular Research Institute, Massachussets General Hospital, Charlestown, MA, USA [17]Section of Computational Biomedicine, Department of Medicine, Boston University School of Medicine, Boston, MA, USA [18]Thoracic Aortic Center, Division of Cardiology, Massachusetts General Hospital, Harvard Medical School, Boston, MA, USA [19]Cardiovascular Research Center, Division of Cardiology, Massachusetts General Hospital, Harvard Medical School, Boston, MA, USA [20]Division of Cardiovascular and Thoracic Surgery, Duke University Medical Center, Durham, North Carolina [21]Thoracic Aortic Center and Cardiovascular Genetics Program, Division of Cardiology, Massachusetts General Hospital, Harvard Medical School, Boston, MA, USA [22]A list of members of affiliations appears at the end of the paper [23]Division of Cardiology, The Hospital for Sick Children, Labatt Family Heart Centre, Toronto, Ontario, Canada [24]Department of Molecular Medicine and Surgery, University Hospital Solna, Karolinska Institutet, Stockholm, Sweden [25]Department of Clinical Genetics, Erasmus MC, University Medical Center Rotterdam, Rotterdam, The Netherlands [26]Department of Pediatrics, Hospital for Sick Children, University of Toronto, Toronto, Ontario, Canada [27]Department of Human Genetics, Radboud University Medical Centre, Nijmegen, The Netherlands [28]Department of Pediatrics, Université de Montréal, Montreal, Quebec, Canada [29]Department of Pediatrics, Division of Pediatric Cardiology, Johns Hopkins University School of Medicine, Baltimore, Maryland, USA [30]Department of Medicine, Johns Hopkins University School of Medicine, Baltimore, Maryland, USA

[#] These authors contributed equally to this work.

Abstract

Bicuspid aortic valve (BAV) is a common congenital heart defect (population incidence, 1–2%)[1–3] that frequently presents with ascending aortic aneurysm (AscAA)[4]. BAV/AscAA shows autosomal dominant inheritance with incomplete penetrance and male predominance. Causative gene mutations are known for ≤1% of nonsyndromic BAV cases with/without AscAA (e.g. *NOTCH1*, *SMAD6*)[5–8], impeding mechanistic insight and development of therapeutic strategies. We report the identification of mutations in *ROBO4*, encoding a factor known to contribute to endothelial performance, that segregate with disease in two families. Targeted sequencing of *ROBO4* revealed enrichment for rare variants in BAV/AscAA probands compared to controls. Targeted silencing of *ROBO4* or mutant ROBO4 expression in endothelial cell lines results in impaired barrier function and a synthetic repertoire suggestive of endothelial-to-mesenchymal transition (EnMT); concordant BAV/AscAA-associated findings are observed in patients and animal models deficient for ROBO4. These data identify a novel endothelial etiology for this common human disease phenotype.

Kindreds segregating BAV/AscAA often exhibit wide variation in cardiovascular manifestations between affected individuals, including complete non-penetrance (skewed toward females), isolated BAV, isolated AscAA, and variable location of the site of ascending aortic dilatation including isolated aortic root aneurysm (i.e. at the sinuses of

Valsalva, AoRA), or more distal ascending aortic aneurysm (DAscAA; collectively AscAA)[9–12]. This observation suggests that BAV and AscAA are both variably penetrant primary manifestations of the same underlying gene defect(s). While enrichment for BAV can be seen in syndromic presentations of thoracic aortic aneurysm (e.g. Loeys-Dietz syndrome caused by mutations in genes encoding primary effectors of the transforming growth factor-β (TGFβ) signaling pathway), isolated DAscAA is exceedingly rare in these conditions suggesting a mechanistic distinction for nonsyndromic BAV/AscAA[13–15]. The genetic etiology and molecular pathogenesis of nonsyndromic BAV/AscAA remains largely elusive despite intensive effort. Likely obstacles to progress include extreme locus heterogeneity and the confounding influence of incomplete penetrance, sex bias, and environmental and/or genetic modification of disease onset and severity. In this study, we sought to identify genes responsible for nonsyndromic BAV/AscAA using whole exome sequencing (WES) and a familial segregation approach.

A total of nine patient families (Fig. 1a,c and Supplementary Fig. 1), 286 individual probands, and 193 unrelated controls without structural heart disease were enrolled in our WES initiative. In one large family (Family 1), eight individuals showed AoRA with or without DAscAA; two had associated BAV (Fig. 1a).

Initial sequencing of a panel of genes implicated in familial thoracic aortic aneurysm (*ACTA2*, *FBN1*, *MYH11*, *MYLK*, *SMAD3*, *TGFBR1/2*)[16–21] identified no mutations. WES in five affecteds of family 1 identified a novel heterozygous mutation at the splice acceptor site of *ROBO4* exon 13 (g.124757628C>A, c.2056+1G>T, denoting the variant position in genomic DNA and complementary DNA, respectively. NC_000011.9 and NM_019055.5) (Fig. 1a and Supplementary Fig. 2a). We confirmed that all eight affected family members carried the mutation. Interestingly, seven of eight affected individuals were male including both with BAV. Two clinically unaffected female family members were heterozygous for the *ROBO4* splice-site mutation. Pathology from one family member with BAV revealed valve thickening in association with a pronounced fibroproliferative process (Supplementary Fig. 2b). Amplification and sequencing of cDNA derived from patient and control fibroblasts showed that the splice-site mutation results in the skipping of the 108 base pairs encoding exon 13 of *ROBO4*, resulting in an in-frame transcript encoding a protein isoform missing 36 amino acids from the intracellular domain (Fig. 1b). In family 2, WES revealed a heterozygous *ROBO4* missense variant (c.190C>T; p.Arg64Cys) in a woman, with atrial septal defect (ASD) and aortic valve stenosis (AVS) that required surgery, and her son with ASD, BAV and significant AVS (Fig. 1c and Supplementary Fig. 2c). This variant is exceedingly rare (ExAC frequency: 19/98,998), predicted deleterious by Polyphen and SIFT, and predicted to be among the 1% most deleterious substitutions possible in the human genome by the Combined Annotation Dependent Depletion (CADD) algorithm (score, 21.6). The mutation substitutes an evolutionarily conserved residue in the Ig-like C2-type 1 extracellular domain of ROBO4. Of the additional 286 individual probands evaluated, four variants (p.Ala95Thr, p.Thr232Met, p.His411Gln and p.Arg568Ter) met our *a priori* filter, restricting our focus to exceedingly rare (MAF<0.01%), or rare and predicted highly deleterious (MAF<0.1% and CADD>20) variants (Fig. 1d and Table 1). All four were confirmed by Sanger sequencing.

We then sequenced an additional 441 probands with BAV/AscAA and 183 unrelated controls, with echocardiogram-confirmed absence of structural cardiovascular disease, for *ROBO4* mutations using the Haloplex target enrichment system (99.47% of *ROBO4* base positions ≥10x coverage in 90% of samples). Seven additional BAV/AscAA probands harbored heterozygous *ROBO4* variants that fulfilled filtering criteria, including five missense mutations and one frameshift mutation (Fig. 1d and Table 1; See Supplementary Table 1 for corresponding clinical data).

The missense mutations observed in the targeted sequencing cohort include an independent example of the p.Arg64Cys variant observed in Family 2. Additionally, we observe an exceedingly rare (ExAC frequency: 4/110,004) and predicted highly deleterious (CADD score 21.3) variant (p.Asp622His) in two unrelated probands, recruited at distant sites. Collectively, among familial and individual probands (WES and targeted sequencing), 13/736 (1.77%) had a *ROBO4* variant that passed *a priori* filtering constraints while one rare (absent from ExAC) missense mutation was observed among 376 rigorously phenotyped controls (Two-tailed Fisher's Exact Test. $P = 0.0432$). Consistent with BAV overall, the majority of BAV/AscAA probands identified with putative pathogenic *ROBO4* variants were male (Supplementary Table 1); the mechanistic basis for this observation is unknown.

We next sought to elucidate the functional consequence of mutant *ROBO4* alleles. Histologic and immunofluorescent analyses were performed on resected ascending aortic aneurysm tissue from patient 1.II:1 and compared to normal ascending aorta derived from an age- and sex-matched control individual. ROBO4 was strongly expressed in endothelial cells in control aorta as evidenced by co-localization with platelet endothelial cell adhesion molecule 1 (CD31) but was diminished in the endothelium in the BAV/AscAA sample (Fig. 2a, c).

Both control and diseased aorta showed expression of ROBO4 in the intima in the absence of co-expression of α-smooth muscle actin (α-SMA), a vascular smooth muscle cell mesenchymal marker (Fig. 2b). However, the aneurysm tissue uniquely showed infiltration of ROBO4+ cells into the aortic media with co-staining for α-SMA. Given ROBO4 expression in the endothelial lining of the vasculature[22] and a described role in establishing endothelial barrier function[23,24], we hypothesized enhanced vascular permeability in the ascending aorta of patients with BAV/AscAA. In keeping with this hypothesis, immunostaining for albumin was restricted to the endothelial surface in control aorta, but substantial penetration into the aortic intima was observed in patient tissue (Fig. 2d). Histologic analyses showed a strong fibroproliferative response in the intima and superficial medial layer of patient aorta, as evidenced by increased cellularity and the accumulation of collagen upon Masson's trichrome staining. Further, decreased elastin content and fragmentation and disarray of elastic fibers in the superficial media was revealed upon Verhoeff-Van Gieson (VVG) staining (Fig. 2e). Collectively, these data suggest that *ROBO4* mutations disrupt endothelial cellular performance and barrier function, contributing to pathological remodeling of the aortic media.

To further address the impact of *ROBO4* mutations on endothelial cell performance, cultured human aortic endothelial cells (HAECs) were transiently transfected with short interfering

RNA (siRNA) against ROBO4 or with constructs overexpressing either wild-type ROBO4, a form lacking exon 13, or a form with the p.Arg64Cys missense variant. Further, to assess the individual performance of the ROBO4 variant seen in Family 1, HAECs with silenced endogenous ROBO4 expression (siRNA targeting sequence in exon 13) were transfected with the expression construct lacking exon 13 (termed SS-Alone). The expression of wild-type and mutant *ROBO4* mRNA was assessed by quantitative reverse transcription-PCR (qRT-PCR) (Fig. 3a).

Either *ROBO4* silencing or expression of ROBO4 variants resulted in loss of endothelial barrier function in a dextran permeability assay (Fig. 3b). Loss of barrier function associated with down regulation of expression of TJP1 and VE-cadherin mRNA and protein, indicative of loss of tight- and adherens-junction integrity, respectively (Fig. 3c). Other phenotypes seen included induction of expression of α-SMA and *Snail1* mRNA and cellular elongation and invasion. Assessment of expression of prototypical target genes suggested a modest decline in bone morphogenetic protein (BMP) and Notch activity without altered TGFβ responses upon ROBO4 silencing. (Supplementary Fig. 3). Together, these results suggest that reduction or structural disruption of ROBO4 compromises endothelial identity and performance, as well as its capacity to suppress transition to a mesenchymal invasive character and synthetic repertoire. These data suggest that loss-of-function (by functional haploinsufficiency or the antimorphic effects of overexpressed mutant protein) is the relevant pathogenic mechanism. The distribution of missense variants along the full length of the gene and protein argues against particular relevance for any domain-specific function such as homo- or heterodimerization, interaction with other binding partners or recruitment of SLIT ligands.

ROBO1, ROBO2, SLIT2 and SLIT3 are expressed in or adjacent to the endocardial cushions and heart valves during mouse development[25]. Targeted homozygous disruption of both *Robo1* and *Robo2* or *Slit3* resulted in highly penetrant septal defects with variably penetrant valve anomalies, including BAV. We observed that mouse ROBO4 was expressed in the endocardial layer of the cushions and delamination zones at embryonic day 11.5 (E11.5; Supplementary Fig. 4a). By E17, ROBO4 was detected in both the endothelial and interstitial cells of the developing aortic valve and endothelial cells of the proximal aorta (Supplementary Fig. 4a, b). At 5 weeks after birth, ROBO4 was localized to the endothelial layer of the ascending aorta and persisted throughout postnatal development (Supplementary Fig. 4b). In normal adult human ascending aorta, ROBO4 is expressed in endothelial and intimal cells (Fig. 2 and Supplementary Fig. 4c). Similarly, robo4 is known to be expressed in the developing vasculature of zebrafish[26]. Together, these results confirm expression of ROBO4 in cells relevant to the pathogenesis of BAV/AscAA.

Next, we established a mutant zebrafish (*Danio rerio*) line harboring a seven-nucleotide deletion in exon 6 of *robo4* (*robo4*$^{\Delta 7}$; Supplementary Fig. 5a). This frameshift mutation leads to a low steady-state abundance of *robo4* mRNA due to nonsense mediated mRNA decay (Supplementary Fig. 5b). We observed no gross defect in robo4 mutant larvae (Supplementary Fig. 6). Among the adult mutant zebrafish assayed by echocardiography, 7/26 (26.9%) *robo4*$^{\Delta 7/+}$ and 4/15 (26.7%) *robo4*$^{\Delta 7/\Delta 7}$ zebrafish displayed regurgitation and/or turbulence across the ventriculo-bulbar valve compared to 4/45 (8.9%) of the wild-

type controls ($P < 0.05$; Supplementary Fig. 5c-e and Supplementary Table 2). Thus, targeted disruption of robo4 in zebrafish perturbs outflow tract function. While overt vascular enlargement was not observed, it is unclear whether the zebrafish system is ideal for assessment of this specific aspect of the phenotype given substantive anatomic and physiologic differences from mammals and the limited duration of observation.

We next examined the effect of ROBO4 loss of function in mice using the *Robo4*^{tm1Lex} model, that lacks exons 1 through 3. *Robo4* transcripts were not detected in homozygous *Robo4*$^{tm1Lex/tm1Lex}$ mice via qRT-PCR (Supplementary Fig. 7a). None of the evaluated heterozygotes (*Robo4*$^{tm1Lex/+}$) presented with any structural or functional abnormality. Homozygous *Robo4*$^{tm1Lex/tm1Lex}$ knockout mice exhibited a complex cardiovascular phenotype that includes a combination of aortic valve thickening with or without BAV, aortic valve stenosis and/or regurgitation and/or AscAA. In general, these phenotypes were observed with low penetrance and male predominance. Overall, at 20 weeks of age, 5/28 (17.9%) male and 2/18 (11.1%) female *Robo4*$^{tm1Lex/tm1Lex}$ mice were affected compared to 0/22 (0%) and 0/19 (0%) *Robo4*$^{+/+}$ males and females, respectively ($P < 0.01$; Fig. 4). Additionally, one mouse with aortic regurgitation presented with a quadricuspid aortic valve (Supplementary Fig. 7b).

We next sought to evaluate the *in vivo* consequence of the splice mutation (g. 124757628C>A, c.2056+1G>T) that we had observed in Family 1 by establishing a knock-in mouse line harboring a mutation (*Robo4*^{Skip13}) at the splice donor site in intron 13 of *Robo4* (c.2089+1G>T) (Supplementary Fig. 8a). Sanger sequencing of cDNA amplicons spanning exons 11–14, using mRNA derived from the ascending aorta of targeted animals, revealed either in-frame skipping of exon 13 (Exons 12/14) or inclusion of exon 13 with activation of a cryptic splice donor in intron 13 (Supplementary Fig. 8b, c). Using TaqMan™ probes specific to individual exons or splice junctions, we determined that wild-type mice show 100% normal splicing (Exons 12/13/14). Representation of Exons 12/13/14, Exons 12/13+Intron 13 and Exons 12/14 transcripts was ~50%, 28% and 22% or ~0%, 55% and 45% in *Robo4*$^{+/Skip13}$ or *Robo4*$^{Skip13/Skip13}$ animals, respectively (Supplementary Fig. 8d). We conclude that the *Robo4*^{Skip13} mutation alters pre-mRNA splicing with significant representation of mature mRNA lacking exon 13.

Like the knockout mice, *Robo4*^{Skip13} mice presented with an incompletely penetrant complex cardiovascular phenotype that included aortic valve defects and aortic valve dysfunction and AscAA. At 20 weeks, 1/31 (3.2%) *Robo4*$^{Skip13/+}$ and 4/35 (11.4%) *Robo4*$^{Skip13/Skip13}$ male mice were affected compared to 0/18 *Robo4*$^{+/+}$ mice ($P < 0.05$; Fig. 5).

We demonstrate that heterozygous mutations in *ROBO4* are sufficient to cause a nonsyndromic presentation of BAV/AscAA. The distribution of expression of ROBO4 in both the developing valve and the ascending aorta is consistent with the view that BAV and aortic aneurysm present as independent primary manifestations of the same underlying gene defect, a concept further supported by the presence of either BAV/AscAA, isolated BAV, or isolated AscAA in family members segregating the same *ROBO4* mutation. This study highlights many obstacles in the elucidation of etiologies for BAV/AscAA including a

relatively low frequency for involvement of any specific disease gene (also evident for *NOTCH1* and *SMAD6*), apparent extreme locus heterogeneity, functional redundancy within relevant pathways, low penetrance with sex bias, and the lack of signature for loss-of-function intolerance that is likely related to both the penetrance issue and to later onset of the phenotype and hence minimal, if any, impact on reproductive fitness. This study focuses attention on endothelial cell biology in BAV/AscAA, with impairment of barrier function and/or dysregulation of mesenchymal transition potentially contributing to disease expression. Prior work has suggested that abnormal plasma protein (e.g. plasminogen) trafficking in the vessel wall might contribute to aneurysm phenotypes by enhancing proteolytic activity, TGFβ bioavailability or other mechanisms[27,28]. Other studies have suggested an association between BAV/AscAA and an EnMT-like phenotype in the aortic wall[29] and decreased mesenchymal potential of endothelial cells derived from such patients[30], but neither study had defined the etiology or mechanism for these findings. While our study of isolated endothelial cells did not reveal a predominant pathway driving apparent EnMT in the context of ROBO4 deficiency, a confluence of data provides further incentive to interrogate altered mesenchymal transition as a pathogenic driver and a therapeutic target in BAV/AscAA using model systems that mimic the anatomic and physiologic complexity of the left ventricular outflow tract and ascending aorta.

METHODS

Study participants.

Affected individuals were recruited from the Connective Tissue Clinic at Johns Hopkins Hospital (H.C.D.), Duke University (G.C.H.), Radboud University Hospital/Antwerp University Hospital (B.L.L.), Centre Hospitalier Universitaire Sainte-Justine (G.A.), Karolinska University Hospital (P.E.), University of Luebeck (S.A.M.), Sickkids Hospital (S.M.), and Erasmus University Medical Center (M.W.) in strict compliance with all relevant ethical regulations. All skin biopsies and research protocols were collected in compliance with the Institutional Review Board at each respective institution after informed consent was obtained. Echocardiograms were performed and interpreted as previously described[31].

Whole exome sequencing.

Genomic DNA was extracted from peripheral blood lymphocytes using standard protocols. DNA fragmentation was performed using a Covaris S2 system, and exon capture was performed using the Agilent SureSelect 38 Mb Human All Exon Target Enrichment system. DNA sequencing was performed on an Illumina Genome Analyzer IIx instrument with using standard protocols for 75 base pair paired-end runs.

Bioinformatics analysis.

Reads were mapped to the human reference genome (UCSC hg19) using the Burrows-Wheeler Aligner (BWA) and a variant list created using SAMtools, which were annotated using ANNOVAR[32–34]. Local realignment and recalibration of base call quality scores was performed using the Genome Analysis Toolkit (GATK)[35,36]. Duplicates were identified using Picard. We selected for rare variants (dbSNP, exome variant server, ExAC) and focused only on exonic non-synonymous, splice-site and insertion and/or deletion (indel)

variants. Variants were viewed directly using the Integrated Genome Viewer (IGV) and excluded if reads were only present in one direction, if ambiguously mapped reads were present, or if an indel occurred within 3 base pairs of the end of the read[37].

Mutation validation and Sanger Sequencing of candidate genes.

Bidirectional Sanger DNA sequencing assays were performed using primers designed 60–120 base pairs from the variants or intron-exon boundaries to confirm candidate variants or sequence candidate genes. PCR was performed using a DNA Engine Dyad thermal cycler (Bio-Rad). Phusion Flash High Fidelity PCR Master Mix was used in accordance with the manufacturer's instructions for each primer set (Thermo Scientific). Cycle sequencing was performed using the BigDye Terminator v3.1 kit and an ABI 3730xl DNA Analyzer in accordance with the manufacturer's instructions (Life Technologies). Samples were purified using the QIAquick PCR Purification kit (Qiagen).

Targeted sequencing.

Enrichment for all exons of *ROBO4*, including ±10 nucleotides of adjacent intronic sequences, was performed with a custom Haloplex target enrichment kit per instructions of the manufacturer (Agilent Technologies, USA). Probe design covered a theoretical 99.7% of the complete target region. Pooled samples were sequenced either on a HiSeq 2500 (Illumina, USA) with 2×150 base pair reads or on a HiSeq 1500 (Illumina, USA) with 2×100 base pair reads.

Cell culture and transfection.

Primary human dermal fibroblasts were derived from forearm skin biopsies from one control individual, a control cell line (ATCC), or a single proband. Cells were cultured in DMEM supplemented with 10% FBS in the presence of antibiotics and were passaged at confluence. Human aortic endothelial cells (HAEC) (Promocell, Heidelberg) were cultured in EGM2 BulletKi (Lonza, CC-3156/CC-4176) and used for experiments at P2-P4. For initial transfection experiments, cells were seeded at 60–70% confluence. *ROBO4* constructs were mixed with Lipofectamine 3000 (Invitrogen), diluted in EGM2 (without antibiotics) (for constructs, see Supplementary Table 5), and treated for 24 hours. HAEC media was then replaced and allowed to culture for an additional 48 hours. Transfection efficiency was measured via qRT-PCR and immunofluorescence.

RNA isolation and qRT-PCR.

For human and mice samples, RNA extractions were performed using a Qiagen total RNA purification kit (Qiagen) and RNA was reverse transcribed to cDNA using the SuperScript III RT-PCR kit with oligo(dT) primer (Invitrogen). Real-time PCR experiments were conducted using the FAM-MGB PCR system (Applied Biosystems) on QuantStudio 7 Real-Time ABI 384 cycler, with 40 cycles per sample. Primers were normalized to 18S or GAPDH. The following pre-validated probes were used for mRNA analysis: H200219408_m1 (*Robo4*), Hs01551861_m1 (*TJP1*), Hs00901463_m1 (*CDH5*), Hs00426835_g1 (*ACTA2*), Hs00195591_m1 (*SNAI1*), Hs00170014_m1 (*CTGF*), Hs00167155_m1 (*SERPINE1),* Hs03676575_s1 (*Id1*), Hs04187239_m1 (Id2),

Hs00954037_g1 (Id3), Hs01114113_m1 (*Hey1),* Hs00232622_m1 (*Hey2),* Hs03003631_g1 (18S), and Hs02758991_g1 (*GAPDH*) (Life technologies). For zebrafish, RNA extracts were prepared from isolated wild-type or *robo4* knockout adult hearts using RNA TRIzol (Ambion) and cDNA was synthesized using SuperScript III Reverse Transcriptase kit (ThermoFisher Scientific). Two sets of specific primers spanning the junctions of exons 9 and 10 and of exons 16 and 17 were designed (see Supplementary Table 5). All qRT-PCR data was obtained using the ViiA 7 Real-Time PCR System (Applied Biosystems) and SYBR Green PCR Mix (ThermoFisher).

Antibody staining.

Samples were fixed in 4% paraformaldehyde overnight at 4°C. Samples were then washed for 15 minutes on a rocker 3 times with PBS, permeabilized with 0.2% Triton-X 100 (VWR International, Radnor, PA) for 10 minutes, and washed another 3 times with PBS. Samples were incubated overnight at 4°C in a 1% BSA (Rockland Immunochemicals) blocking solution followed by another 4°C overnight incubation with ROBO4 (Abcam, ab103674), ROBO4 (Santa Cruz, sc-46497), CD31 (Biocare Medical, CM303A), PECAM1 (Santa Cruz, sc-1506), CDH5 (Santa Cruz, sc-28644), TJP1 (Santa Cruz, sc-8146), ACTA2 (Abcam, ab7817), or ALB (Santa Cruz, sc-46293). After 3 washes for 15 minutes with PBS, samples were exposed to Alexa Fluor 488 or 568 conjugated (Invitrogen), species-specific secondary antibodies at 1:100 in 1% BSA for 2 hours at room temperature. Three more washes with PBS for 15 minutes were followed by incubation with either DRAQ5 (far-red) nuclear stain or DAPI (UV) nuclear stain (Enzo Life Sciences) at 1:1000.

Permeability assay.

Permeability assays were performed as described previously[38]. HAECs were utilized at or before passage six. Cells were detached using 0.05% trypsin-EDTA, pelleted, then re-suspended in a growth medium to a concentration of 0.5–1X at 10^6 cells/mL. Dry collagen pre-coated porous inserts were rehydrated for 15 minutes in a growth medium prior to cell seeding (1.0um pores, EMD Millipore). HAECs were seeded in 200 μL of growth medium per 24 well insert. 500 μL were added to each receiver plate well. HAECs were cultured in a 37°C/5% CO_2 tissue culture incubator for 72 hours to allow for a monolayer formation. Following endothelial monolayer formation, growth medium was carefully removed. This was replaced with medium containing different *ROBO4* constructs (see Supplementary Table 5). Samples were returned to 37°C incubation for 24 hours. Afterwards, the treatment medium was carefully removed. A high molecular weight FITC-dextran solution (40kDA) was created by 1:40 dilution in a growth medium and added at 150 μL. Growth medium was added to each receiver plate well at 500 μL (24-well). The FITC-dextran permeated the monolayers for 2 hours. The inserts were removed from the receiver wells to stop permeation. The medium in the receiver wells was then thoroughly mixed and 100 μL was removed from each well to a black 96-well opaque plate for fluorescence measurement. Permeability was quantified on a Synergy-II fluorescent plate reader (Biotek) via fluorescence at 485nm excitation/535nm emission wavelengths (1 second fluorescent count time). The endothelial monolayer was stained after completion of FITC-dextran permeability testing for subsequent confocal imaging.

Cell morphology assay.

Cell shape was calculated as previously described[39] using ImageJ (https://imagej.nih.gov/ij/plugins/circularity.html). Cell shape changes were automatically tracked over subsequent images, and quantified as a cell circularity index (CI = 4*Pi*(Area/Perimeter2)). A circularity value of 1.0 indicates a perfect circle. As the value approaches 0.0, it indicates an increasingly elongated polygon.

Endothelial aggregate invasion assay.

For invasion assays, cells were re-suspended in culture media and allowed to aggregate overnight in hanging drop culture (20 μL; 20,000 cells). The aggregates were then placed on the surface of neutralized type I collagen hydrogels (1.5 mg/mL) as previously described[40] and allowed to adhere for 2 hours before adding treatments. Cultures were then transfected for 24 hours with the *ROBO4* constructs (see Supplementary Table 5) and maintained for another 72 hours. Cell invasion was quantified manually at a 50-μm depth into the gel and normalized to control.

Proliferation assay.

5-bromo-2′-deoxyuridine (BrdU) incorporation was used to detect proliferating cells as described previously[41]. Cultures were transfected for 24 hours with the *ROBO4* constructs (see Supplementary Table 5). BrdU labeling reagent (Invitrogen) was added to the culture media for 12 hours after treatment. After 24 hours, cells were fixed and targeted with a monoclonal Anti-BrdU Alexa Fluor 488 conjugate (PRB-1, Invitrogen) while total DNA was counterstained using a DAPI dye. Positive fluorescent areas for each cell were measured using ImageJ and normalized by cell nuclei.

Scratch assay.

Migratory ability was tested as described previously[42]. Briefly, cells were cultured to confluency and then transfected for 24 hours with the *ROBO4* constructs. A scratch was then introduced using a 200-μl pipette tip. The cells were then incubated at 37°C and observed at 24 hours. Differences in filling in the scratch were observed to establish the capability of cellular migration.

Zebrafish and mouse maintenance.

Adult AB and *robo4*$^{\Delta 7}$ mutant zebrafish lines were maintained in system water according to standard methods[43]. Mice were housed in the Johns Hopkins University School of Medicine East Baltimore campus. All strains were maintained on a mixed C57BL/6J and F129/SVE background. All zebrafish and mice upkeep and experimental procedures were in accordance with the ethical permits set by the Johns Hopkins Institutional Animal Care and Use Committee.

Generation of a *robo4* knockout zebrafish line by CRISPR/Cas9.

We designed a single guide RNA (gRNA, see sequences in Supplementary Table 6) to target the *robo4* gene (gRNA^{robo4}), using ZiFit[44,45]. Cas9 RNA was synthesized from linearized pCS2-nls-zCas9-nls (AddGene, no. 47929)[46]. We injected 100 ng/nL of gRNA and 300 ng

of Cas9 in a 5-μL solution into 1-cell wild-type (AB) zebrafish embryos and raised them to maturity (F_0). To identify fish capable of germline transmission, we crossed F_0 males with AB females. Germline transmission was confirmed by Surveyor Assay (IDT) in pooled F_1 embryos ($n = 50$) followed by Sanger sequencing. Heterozygous F_1 adults with the same seven base pair deletion were inbred to establish the line (*robo4*^{jh176}). All subsequent generations were genotyped using primer set F2 and R2 (see Supplementary Table 6).

Robo4 knockout mice and generation of *Robo4* knock-in mice.

Robo4^{tm1Lex} knockout mice were purchased through the mutant mouse resource and research centers supported by the NIH (MGI:5007309, Lexicon Pharmaceuticals). The mice were bred in a heterozygous state on a mixed background of 129S5/SvEvBrd and C57BL6/J. To generate *Robo4* knock-in mice, we targeted the *Robo4* locus using CRISPR/Cas9. Two single-guide RNA (sgRNA) sequences (see Supplementary Table 7) were designed to target exon 13 of *Robo4* (NC_000074.5) using a gRNA CRISPR design tool (http://crispr.technology/)47. Neither gRNA was predicted to have any off-target effects. These oligonucleotides were cloned into a pX459 plasmid[48] (Addgene, no. 48139) and appended with a T7 promoter. The sgRNA was transcribed in vitro. The homology directed repair (HDR) template was purchased as a 4nm Ultramer (IDT, see Supplementary Table 6). The sgRNA, Cas9 (TriLink BioTechnologies), and HDR were co-injected into C57BL/6J zygotes (Johns Hopkins University Transgenic Core). Pups ($n = 41$) were screened for locus editing by Sanger sequencing (IDT, see Supplementary Table 7). Mice (*Robo4*^{Skip13}) were subsequently genotyped by Sanger sequencing (271 base pair amplicon). Mice were then crossed to a mixed background (129S5/SvEvBrd and C57BL6).

Zebrafish and mice echocardiography.

For zebrafish, we used the Vevo 2100 Imaging System equipped with a 70 MHz ultrasound transducer (VisualSonics®, Toronto, ON, Canada). The zebrafish were anesthetized by placing the fish into a plastic cup filled with 100 ml of 168 μg/ml MS-222 (Tricaine methanesulfonate, Fluka Analytical). For mice, echocardiograms were undertaken on awake, unsedated mice using the Vevo 2100 Imaging System (VisualSonics®, Toronto, ON, Canada) and a 40 MHz transducer. Echocardiographic recordings for the mice were taken using a parasternal long-axis or sagittal short axis view; 3 independent measurements of the maximal internal dimension at the sinus of Valsalva and ascending aorta were made and averaged. All data acquisition and measurements for mice and zebrafish were performed blinded to the genotype.

Statistics and reproducibility

For experiments including multiple comparisons, *P* values refer to one-way ANOVA followed by Tukey's post-hoc test. For experiments including only one comparison, *P* values refer to unpaired two-tailed Student's *t*-test, two-tailed Welch's *t*-test, or two- or one-tailed Fisher's exact test. *P* values less than 0.05 were considered significant. *P* values are provided as exact figures where possible, otherwise reported as a range when a large amount of comparisons were performed in a single figure or panel. Data are shown as mean ± standard error (SE) or standard deviation (SD). Further information on experimental design and reagents can be seen in the Life Sciences Reporting Summary

Supplementary Material

Refer to Web version on PubMed Central for supplementary material.

ACKNOWLEDGEMENTS

The authors gratefully acknowledge support from the Leducq Foundation to A.S.M. and H.C.D., from NHGRI (1U54HG006542) to D.V. and J.L., from NHLBI (HL110328, HL128745) and NIH (S10OD012287) to J.T.B. We also thank the American Philosophical Society for support of H.A. through the Daland Fellowship. Additionally, we thank Johns Hopkins University School of Medicine, McKusick Nathans Institute of Genetic Medicine Center for Functional Investigation in Zebrafish (FINZ) for their technical support and to Corinne Boehm for her assistance in depositing variant information to ClinVar. B.L.L. is senior clinical investigator of the Fund for Scientific Research, Flanders and holds a starting grant from the European Research Council (ERC-StG-2012–30972-BRAVE). A.V. is a postdoc researcher supported by the Fund for Scientific Research Flanders. I.L. is supported by a PhD grant from the Agency for Innovation by Science and Technology (IWT). M.E.L. is supported by the Toomey Fund for Aortic Dissection Research and the Fredman Fellowship in Aortic Disease. G.A. is a FQRS Senior Clinical Research Fellow.

REFERENCES

1. Fedak PWM et al. Clinical and pathophysiological implications of a bicuspid aortic valve. Circulation 106, 900–904 (2002). [PubMed: 12186790]
2. Mack G & Silberbach M Aortic and pulmonary stenosis. Pediatr. Rev 21, 79–85 (2000). [PubMed: 10702320]
3. Ward C Clinical significance of the bicuspid aortic valve. Heart 83, 81–85 (2000). [PubMed: 10618341]
4. Tadros TM, Klein MD & Shapira OM Ascending aortic dilatation associated with bicuspid aortic valve. Pathophysiology, molecular biology, and clinical implications. Circulation (2009). doi: 10.1161/CIRCULATIONAHA.108.795401
5. Cripe L, Andelfinger G, Martin LJ, Shooner K & Benson DW Bicuspid aortic valve is heritable. J. Am. Coll. Cardiol 44, 138–143 (2004). [PubMed: 15234422]
6. Garg V et al. Mutations in NOTCH1 cause aortic valve disease. Nature 437, 270–274 (2005). [PubMed: 16025100]
7. McKellar SH et al. Novel NOTCH1 mutations in patients with bicuspid aortic valve disease and thoracic aortic aneurysms. J. Thorac. Cardiovasc. Surg 134, 290–6 (2007). [PubMed: 17662764]
8. Tan HL et al. Nonsynonymous variants in the SMAD6 gene predispose to congenital cardiovascular malformation. Hum. Mutat 33, 720–727 (2012). [PubMed: 22275001]
9. Clementi M, Notari L, Borghi A & Tenconi R Familial congenital bicuspid aortic valve: A disorder of uncertain inheritance. Am. J. Med. Genet 62, 336–338 (1996). [PubMed: 8723060]
10. Huntington K, Hunter AGW & Chan KL A prospective study to assess the frequency of familial clustering of congenital bicuspid aortic valve. J. Am. Coll. Cardiol 30, 1809–1812 (1997). [PubMed: 9385911]
11. Mckusick VA, Logue RB & Bahnson HT Association of Aortic Valvular Disease and Cystic Medial Necrosis of the Ascending Aorta. Circulation 16, 188–194 (1957). [PubMed: 13447162]
12. Loscalzo ML et al. Familial thoracic aortic dilation and bicommissural aortic valve: A prospective analysis of natural history and inheritance. Am. J. Med. Genet. Part A 143, 1960–1967 (2007).
13. Isselbacher EM Thoracic and abdominal aortic aneurysms. Circulation 111, 816–828 (2005). [PubMed: 15710776]
14. Williams JA et al. Early Surgical Experience With Loeys-Dietz: A New Syndrome of Aggressive Thoracic Aortic Aneurysm Disease. Ann. Thorac. Surg 83, (2007).
15. Van Hemelrijk C, Renard M & Loeys B The Loeys-Dietz syndrome: an update for the clinician. Curr. Opin. Cardiol 25, 546–551 (2010). [PubMed: 20838339]
16. Guo D-C et al. Mutations in smooth muscle alpha-actin (ACTA2) lead to thoracic aortic aneurysms and dissections. Nat. Genet 39, 1488–1493 (2007). [PubMed: 17994018]

17. Pereira L et al. Targetting of the gene encoding fibrillin-1 recapitulates the vascular aspect of Marfan syndrome. Nat Genet 17, 218–222 (1997). [PubMed: 9326947]
18. Zhu L et al. Mutations in myosin heavy chain 11 cause a syndrome associating thoracic aortic aneurysm/aortic dissection and patent ductus arteriosus. Nat. Genet 38, 343–349 (2006). [PubMed: 16444274]
19. Wang L et al. Mutations in myosin light chain kinase cause familial aortic dissections. Am. J. Hum. Genet 87, 701–707 (2010). [PubMed: 21055718]
20. van de Laar IMBH et al. Phenotypic spectrum of the SMAD3-related aneurysms-osteoarthritis syndrome. J. Med. Genet 49, 47–57 (2012). [PubMed: 22167769]
21. Loeys BL et al. Aneurysm syndromes caused by mutations in the TGF-beta receptor. N. Engl. J. Med 355, 788–798 (2006). [PubMed: 16928994]
22. Park KW et al. Robo4 is a vascular-specific receptor that inhibits endothelial migration. Dev. Biol 261, 251–267 (2003). [PubMed: 12941633]
23. Jones C. a et al. Robo4 stabilizes the vascular network by inhibiting pathologic angiogenesis and endothelial hyperpermeability. Nat. Med 14, 448–453 (2008). [PubMed: 18345009]
24. Cai H et al. Roundabout 4 Regulates Blood-Tumor Barrier Permeability Through the Modulation of ZO-1, Occludin, and Claudin-5 Expression. J. Neuropathol. Exp. Neurol 74, 25–37 (2015). [PubMed: 25470344]
25. Mommersteeg MTM, Yeh ML, Parnavelas JG & Andrews WD Disrupted Slit-Robo signalling results in membranous ventricular septum defects and bicuspid aortic valves. Cardiovasc. Res 106, 55–66 (2015). [PubMed: 25691540]
26. Bedell VM et al. Roundabout4 Is Essential for Angiogenesis in Vivo. Proc. Natl. Acad. Sci. U. S. A 102, 6373–8 (2005). [PubMed: 15849270]
27. Carmeliet P et al. Urokinase-generated plasmin activates matrix metalloproteinases during aneurysm formation. Nat Genet. 17(4), 439–444 (1997). [PubMed: 9398846]
28. Borges LF. et al. Fibrinolytic activity is associated with presence of cystic medial degeneration in aneurysms of the ascending aorta. Histopathology 57(6), 917–932 (2010). [PubMed: 21166705]
29. Maleki S et al. Mesenchymal state of intimal cells may explain higher propensity to ascending aortic aneurysm in bicuspid aortic valves. Sci. Rep. 6, 35712 (2016). [PubMed: 27779199]
30. Kostina AS et al. Notch-dependent EMT is attenuated in patients with aortic aneurysm and bicuspid aortic valve. Biochim. Biophys. Acta - Mol. Basis Dis 1862, 733–740 (2016).
31. Brooke BS et al. Angiotensin II blockade and aortic-root dilation in Marfan's syndrome. N. Engl. J. Med 358, 2787–95 (2008). [PubMed: 18579813]
32. Li H & Durbin R Fast and accurate short read alignment with Burrows-Wheeler transform. Bioinformatics 25, 1754–1760 (2009). [PubMed: 19451168]
33. Li H et al. The Sequence Alignment / Map format and SAMtools. Bioinformatics 25, 2078–2079 (2009). [PubMed: 19505943]
34. Wang K, Li M & Hakonarson H ANNOVAR: functional annotation of genetic variants from high-throughput sequencing data. Nucleic Acids Res. 38, e164 (2010). [PubMed: 20601685]
35. McKenna A et al. The genome analysis toolkit: A MapReduce framework for analyzing next-generation DNA sequencing data. Genome Res. 20, 1297–1303 (2010). [PubMed: 20644199]
36. DePristo M. a. et al. A framework for variation discovery and genotyping using next- generation DNA sequencing data. Nat Genet 43, 491–498 (2011). [PubMed: 21478889]
37. Robinson JT et al. Integrative genomics viewer. Nat. Biotechnol. 29, 24–26 (2011). [PubMed: 21221095]
38. Anderl J, Ma J & Armstrong L Improved Assays for Quantification of In Vitro Vascular Permeability. 10–14 doi:10.1038/an8623
39. Gould RA et al. Multi-Scale Biomechanical Remodeling in Aging and Genetic Mutant Murine Mitral Valve Leaflets: Insights into Marfan Syndrome. PLoS One 7, (2012).
40. Chiu Y-N, Norris R. a, Mahler G, Recknagel A & Butcher JT. Transforming growth factor β, bone morphogenetic protein, and vascular endothelial growth factor mediate phenotype maturation and tissue remodeling by embryonic valve progenitor cells: relevance for heart valve tissue engineering. Tissue Eng. Part A 16, 3375–3383 (2010). [PubMed: 20629541]

41. Gould RA et al. Cyclic strain anisotropy regulates valvular interstitial cell phenotype and tissue remodeling in three-dimensional culture. Acta Biomater. 8, 1710–1719 (2012). [PubMed: 22281945]

42. Liang C-CC, Park AY & Guan J-LL In vitro scratch assay: a convenient and inexpensive method for analysis of cell migration in vitro. Nat. Protoc. 2, 329–333 (2007). [PubMed: 17406593]

43. Westerfield M The Zebrafish Book A Guide for the Laboratory Use of Zebrafish (Danio rerio), 5th Edition. Univ. Oregon Press Eugene (2007).

44. Sander JD, Zaback P, Joung JK, Voytas DF & Dobbs D Zinc Finger Targeter (ZiFiT): An engineered zinc finger/target site design tool. Nucleic Acids Res. 35, W599–W605 (2007). [PubMed: 17526515]

45. Sander JD et al. ZiFiT (Zinc Finger Targeter): An updated zinc finger engineering tool. Nucleic Acids Res. 38, W462–W468 (2010). [PubMed: 20435679]

46. Jao L-E, Wente SR & Chen W Efficient multiplex biallelic zebrafish genome editing using a CRISPR nuclease system. Proc. Natl. Acad. Sci. U. S. A 110, 13904–9 (2013). [PubMed: 23918387]

47. Jaskula-Ranga V & Zack DJ grID: A CRISPR-Cas9 guide RNA Database and Resource for Genome-Editing bioRxiv (2016).

48. Ran FA et al. Genome engineering using the CRISPR-Cas9 system. Nat. Protoc 8, 2281–2308 (2013). [PubMed: 24157548]

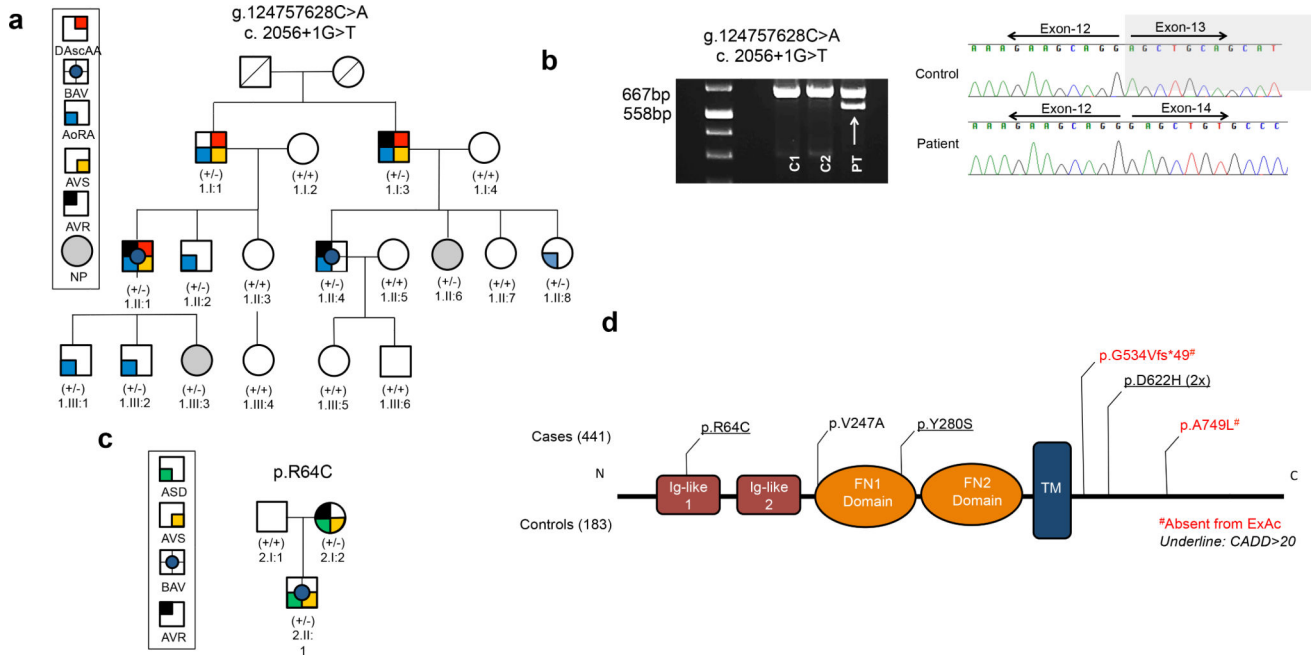

Figure 1.

Identification of *ROBO4* variants segregating in families with bicuspid aortic valve and aortic aneurysms. (**a**) Whole exome sequencing (WES) revealed segregation of a heterozygous obligate splice site mutation (g.124757628C>A, c.2056+1G>T) in a multigenerational family. (**b**) cDNA amplicons spanning exons 11–14 were analyzed from patient (proband 1.II:4) and control fibroblasts. Sanger sequencing confirmed skipping of exon 13 (108 base pair). (**c**) A missense mutation (p.Arg64Cys) was observed in a small family. The missense mutation resides at the Ig-like C2-type-1 (extracellular domain). (**d**) Sequencing of 736 individuals with BAV/TAA and 376 controls. Eleven rare mutations (MAF<0.1% with CADD>20 or MAF<0.01%) were identified in 13/736 patients and one in 1/376 controls (p.Asp510Val). AscAA: ascending aortic aneurysm, BAV: bicuspid aortic valve, AoRA: aortic root aneurysm, AVS: aortic valve stenosis, ASD: atrial septal defect, AVR: aortic valve replacement, NP: non-penetrant

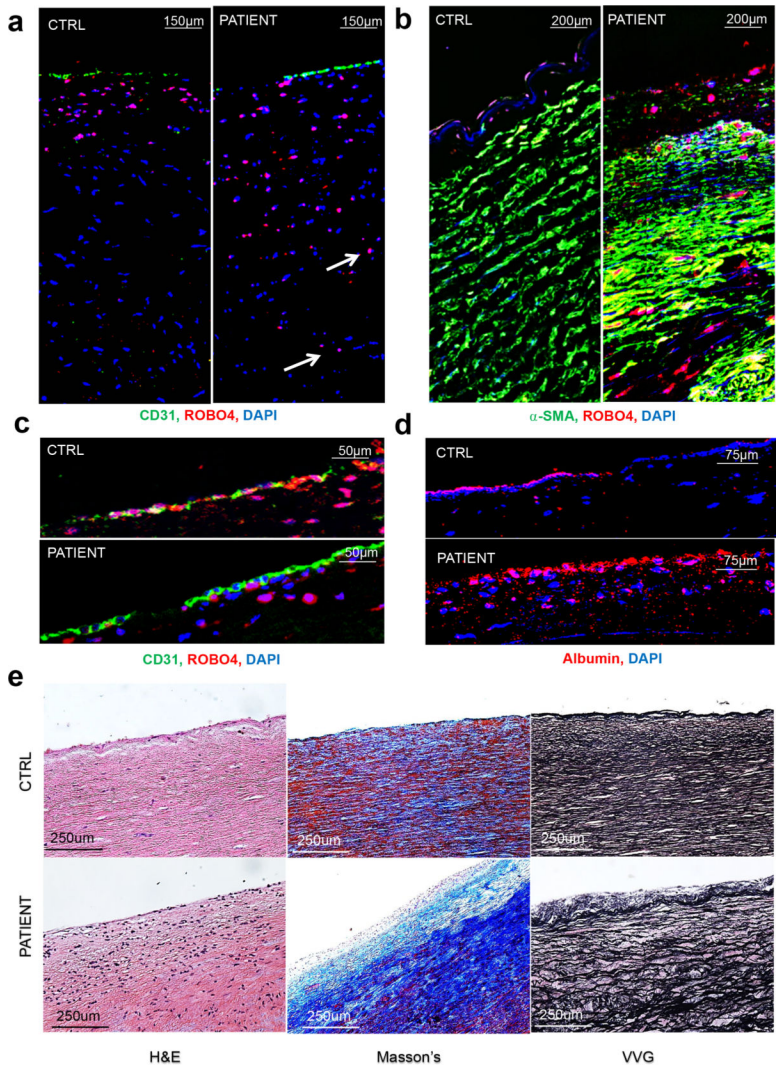

Figure 2.

Evaluation of ascending aortic aneurysm tissue resected from patient 1.II:1, compared to an age- and sex-matched control. (**a**) Immunofluorescent staining of CD31 (green), ROBO4 (red), and DAPI (blue) at the intima-media interface. Arrows indicate ROBO4+ cells deep within the aortic media. (**b**) Immunofluorescent staining of α-SMA (green), ROBO4 (red), and DAPI (blue) at the intima-media interface. (**c**) Immunofluorescent staining of CD31 (green), ROBO4 (red), and DAPI (blue) at the endothelial layer. (**d**) Immunofluorescent staining of albumin (red) and DAPI (blue) at the luminal surface. (**e**) Histological staining (H&E, Masson's, and VVG) of patient and control ascending aortic tissue. VVG: Verhoeff-Van Gieson

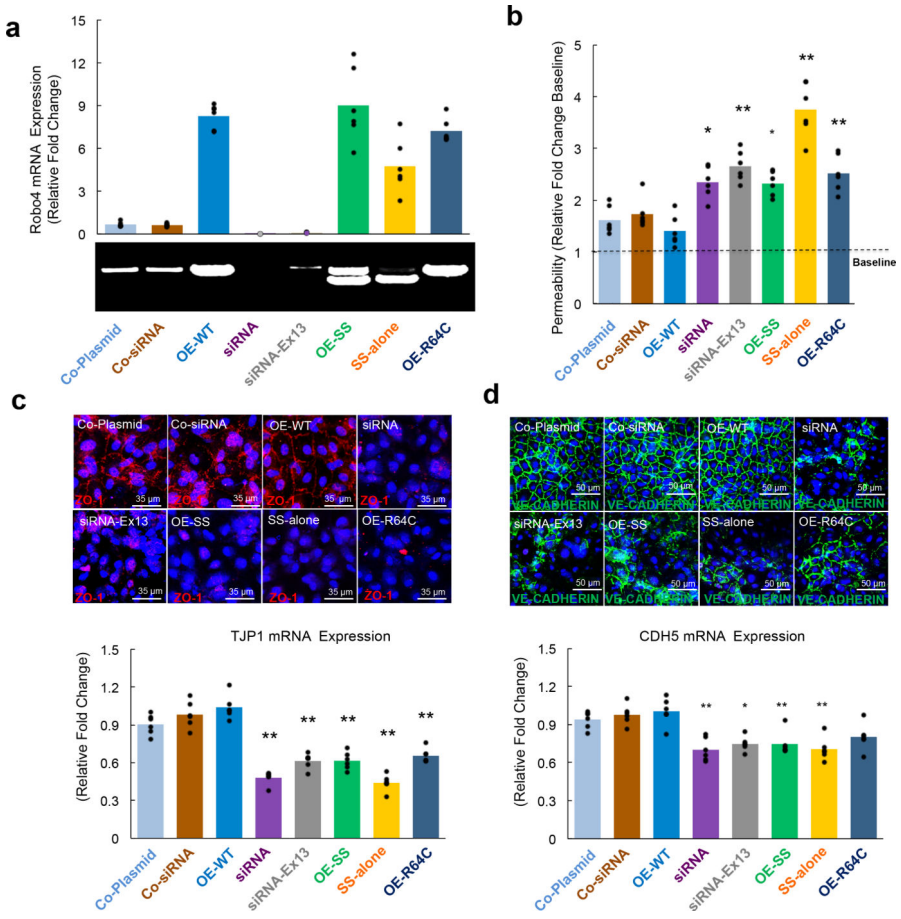

Figure 3.

ROBO4 mutant alleles impair endothelial barrier function. (**a**) HAECs were transfected with either co-plasmid (control GFP plasmid), co-siRNA (control siRNA), OE-WT (overexpression of ROBO4 wild-type plasmid), siRNA (global ROBO4 knockdown), siRNA-Ex13 (ROBO4 knockdown through targeting of exon 13), OE-SS (overexpression of ROBO4 cDNA plasmid without exon 13), SS-alone (overexpression of ROBO4 cDNA plasmid without exon 13 plus silencing of endogenous ROBO4 using siRNA targeting exon 13), OE-R64C (overexpression of ROBO4 cDNA plasmid with p.Arg64Cys) and *ROBO4* mRNA expression was quantified. (**b**) HAECs were cultured to confluency and a dextran permeability assay was used to assess the integrity of the endothelial barrier. Error bars show mean ± SE, $n = 6$. Asterisks signify significant differences per one-way ANOVA with Tukey's Post-hoc (D.F.=7), $*P < 0.05$, $**P < 0.01$. (**c,d**) Immunofluorescent staining of tight junction protein ZO-1 (red), VE-cadherin (green) and DAPI (blue). *TJP1* (encoding tight junction protein ZO-1) expression and *CDH5* (encoding VE-cadherin) expression were analyzed via qRT-PCR. For both **a c and d**, error bars show mean ±SD, $n = 6$. Asterisks signify significant differences per a one-way ANOVA with Tukey's Post-hoc (D.F.=7), $*P < 0.05$, $**P < 0.01$.

a

	Robo4$^{+/+}$		Robo4$^{+/tm1Lex}$		Robo4$^{tm1Lex/tm1Lex}$		
	Male	Female	Male	Female	Male	Female	WT vs. KO
Regurgitation	0/22	0/19	0/14	0/11	4/28	1/18	P=0.037
Flow >600mm/s	0/22	0/19	0/14	0/11	5/28	1/18	P=0.019
AscAA (Z>2)	0/22	0/19	0/14	0/11	3/28	0/18	P=0.143
AoRA (Z>2)	0/22	0/19	0/14	0/11	2/28	0/18	P=0.277
Total Affected	0/22	0/19	0/14	0/11	5/28	2/18	P=0.009
AoV Defect*	0/3	N/A	N/A	N/A	5/5	2/2	P=0.008
Pure BAV**	0/25	N/A	N/A	N/A	1/41	N/A	P=0.627

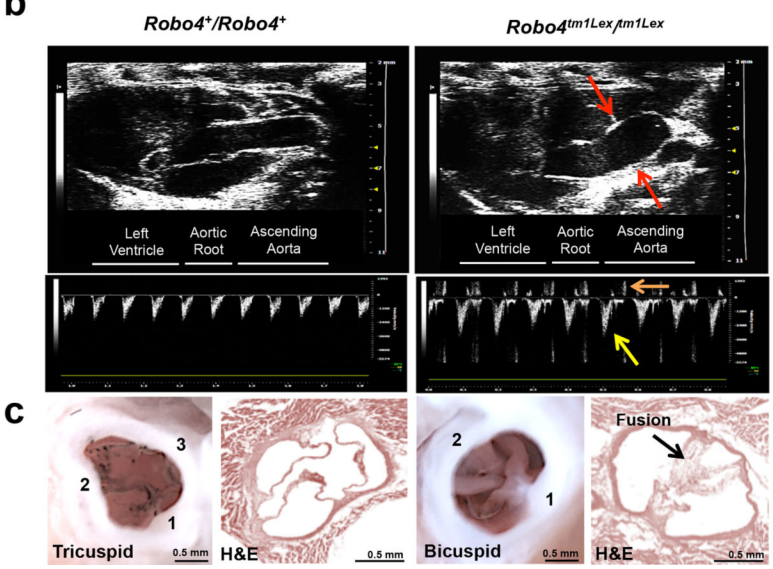

Figure 4.

Robo4 knockout causes aortic valve defects and aortic aneurysm in mice. (**a**) Wild-type (*Robo4*$^{+/+}$), heterozygous (*Robo4*$^{+/tm1Lex}$), and knockout (*Robo4*$^{tm1Lex/tm1Lex}$) mice were aged to 20 weeks and the cardiovascular phenotype was determined. Aortic dilatation was defined as a Z-score greater than two when compared to wild-type male mice by echocardiography. Statistical differences per a one-tailed Fisher's exact test, $n = 112$ total male and female mice, $P < 0.05$ was considered statistically significant. (**b**) Representative parasternal long axis and pulsed-wave Doppler images. Red arrows indicate a dilated segment of the ascending aorta. The yellow arrow shows increased velocity of outflow across the aortic valve during systole while the orange arrow shows regurgitant flow during diastole in a *Robo4*$^{tm1Lex/tm1Lex}$ mouse (similar patterns were seen in the seven affected mice). (**c**) Gross and histological examination of the aortic valve. Numbers refer to individual commissures. AscAA: ascending aortic aneurysm, AoRA: aortic root aneurysm, *abnormal aortic valve morphology including BAV, distal commissure fusion, leaflet thickening, or quadricuspid aortic valve among mutant mice with flow abnormalities by echocardiogram. Comparison is made to a representative sample of wild-type mice. **pure bicommissural aortic valve that was definitively evident by gross inspection. See Supplementary Table 3 for raw data.

a

	Robo4$^{+/+}$ Male	*Robo4*$^{+/Skip13}$ Male	*Robo4*$^{Skip13/Skip13}$ Male	WT vs. HOM
Regurgitation	0/40	1/31	2/35	P=0.214
Flow >600mm/s	0/40	1/31	4/35	P=0.043
AscAA (Z>2)	0/40	1/31	1/35	P=0.467
AoRA (Z>2)	0/40	0/31	1/35	P=0.467
Total Affected	0/40	1/31	4/35	P=0.043
AoV Defect*	0/3	1/1	4/4	P=0.029
Pure BAV**	0/25	0/27	3/43	P=0.246

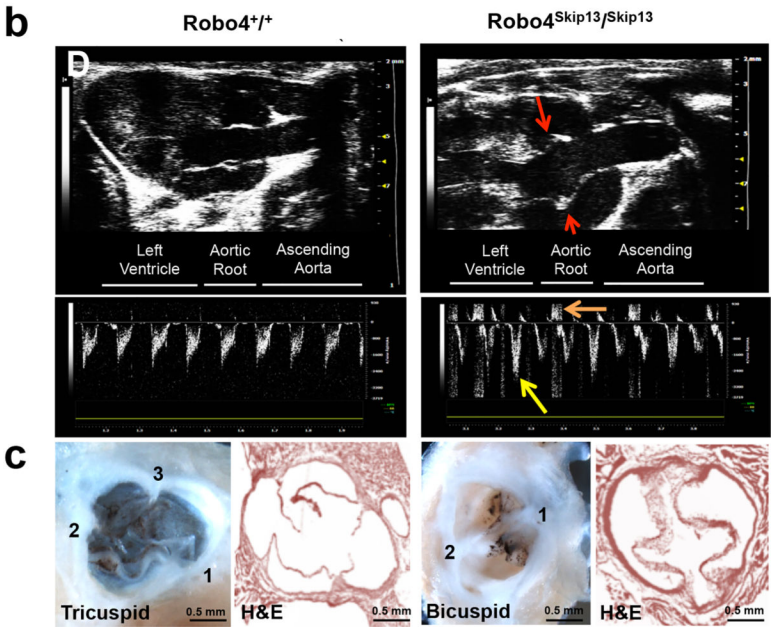

Figure 5.

Knock-in splice site mutation (c.2089+1G>T; *Robo4*^{Skip13}) causes aortic valve defects and aortic aneurysm in mice. (**a**) Wild-type (*Robo4*$^{+/+}$), heterozygous (*Robo4*$^{+/Skip13}$), and homozygous (*Robo4*$^{Skip13/Skip13}$) mice were aged to 20 weeks and the cardiovascular phenotype was determined. Aortic dilatation was defined as a Z-score greater than two when compared to wild-type male mice by echocardiography. Significant differences per a one-tailed Fisher's exact test, $n = 106$ total male mice, $P < 0.05$ was considered statistically significant. (**b**) Representative parasternal long axis and pulsed-wave Doppler images. Red arrows indicate a dilated segment of the aortic root. The yellow arrow shows increased velocity of outflow across the aortic valve during systole while the orange arrow shows regurgitant flow during diastole in a *Robo4*^{Skip13} mouse (similar patterns were seen in the five affected mice).. (**c**) Gross and histological examination of the aortic valve. Numbers refer to individual commissures. AscAA: ascending aortic aneurysm, AoRA: aortic root aneurysm. *abnormal aortic valve morphology including BAV, distal commissure fusion, leaflet thickening, or quadricuspid aortic valve among mutant mice with flow abnormalities by echocardiogram. Comparison is made to a representative sample of wild-type mice. **pure bicommissural aortic valve that was definitively evident by gross inspection. See Supplementary Table 4 for raw data.

Table 1.

ROBO4 variants are more frequent in cases than in controls

WES Families	Variant	Verification		Domain	Fusion pattern	Family history	ExAC	CADD
BAV/AscAA	g.124757628C>Ac.2056+1 G>T	Sanger		/	R-N	Yes	Absent	17.6
BAV/AscAA	c.190C>Tp.Arg64Cys	Sanger		IG-L 1	L-R	Yes	19/98998	21.6
WES Probands	**Variant**	**Depth Allele 1**	**Depth Allele 2**	**Domain**	**Fusion pattern**	**Family history**	**ExAC**	**CADD**
BAV/AscAA	c.283G>Ap.Ala95Thr	7	6	IG-L 1	R-N	No	5/117304	6.42
BAV/AscAA	c.695C>Tp.Thr232Met	42	36	/	R-L	Yes	10/121068	19.56
BAV/AscAA	c.1233T>Ap.His411Gln	31	30	FN2	R-N	Yes	Absent	0.002
BAV/AscAA	c.1702C>Tp.Arg568Ter	43	49	/	R-L	No	12/120920	N/A
Resequencing Probands	**Variant**	**Depth Allele 1**	**Depth Allele 2**	**Domain**	**Fusion pattern**	**Family history**	**ExAC**	**CADD**
BAV/AscAA	c.190C>Tp.Arg64Cys	63	69	IG-L 1	L-R	Yes	19/98998	21.6
BAV/AscAA	c.740T>Cp.Val247Ala	1204	1187	/	L-R	N/A	1/121370	10.5
BAV/AscAA	c.839A>Cp.Tyr280Ser	590	469	FN1	R-N	N/A	5/117546	22
BAV/AscAA	c.1601_1614delp.Gly534Glufs*49	124	114	/	N/A	Yes	Absent	N/A
BAV/AscAA	c.1864G>Cp.Asp622His	767	721	/	L-R	N/A	4/110004	21.3
BAV/AscAA	c.1864G>Cp.Asp622His	1300	1118	/	L-R	No	4/110004	21.3
BAV/AscAA	c.2245_2246delinsCT p.Ala749Leu	195	173	/	R-N	N/A	Absent	16.7
Controls	**Variant**	**Depth Allele 1**	**Depth Allele 2**	**Domain**	**Fusion pattern**	**Family history**	**ExAC**	**CADD**
Control	c.1529A>Tp.Asp510Val	69	51	/	N/A	N/A	Absent	11.6